Journal of Engineering Science and Technology Review 17 (3) (2024) 71-78

Research Article

JOURNAL OF
Engineering Science and Technology Review

www.jestr.org

Evaluation Classification of Weathering Degree of Stone Cultural Relics by Infrared Thermal Imaging

Chengze Ye[1], Zhongfu Qin[2,*], Zhuoyang Shen[1] and Fangze Wang[1]

[1] *ZJU-UIUC Institute, Zhejiang University, Haining 314499, China*
[2] *College of Civil Engineering and Architecture, Zhejiang University, Hangzhou 310058, China*

Received 14 February 2024; Accepted 30 April 2024

Abstract

It is very important to reveal the weathering characteristics of stone cultural relics to protect their integrity for a long time. Infrared thermal imaging was employed in this study to analyze the degree of weathering and classification of stone cultural relics for the protection of the cultural relics. To explore the feasibility of evaluating the overall weathering degree of rock surface, the weathering degree of the rock surface was first determined by using various conventional testing methods. Then, the weathering degree of rock surface was quantified by applying infrared thermal imaging. Finally, the weathering degree of the rock surface was analyzed by comparing it with conventional testing results. Results show that, the infrared thermal imaging can distinguish general disease types and degrees of development based on abnormal surface temperature. When the surface weathering of stone cultural relics is more serious, the temperature change at a certain time is greater after water spraying and cooling. The conclusions obtained in this study can provide a reference for evaluating the overall weathering degree of the surface layer of stone cultural relics via infrared thermal imaging.

Keywords: Stone relics, Nondestructive testing, Infrared thermal imager, Surface weathering

1. Introduction

Given their historical significance and artistic value, stone cultural relics have attracted attention from various aspects of life. To preserve the original historical appearance of these cultural relics as much as possible, many conventional means of detection are inapplicable. With the continuous improvement in science and technology, various methods, including ground-penetrating radar, ultrasonic testing, infrared thermography, and other emerging nondestructive testing techniques are increasingly being applied to the initial investigation and detection of damage in cultural relics.

Existing nondestructive testing methods for the weathering degree of stone cultural relics have become diverse. Among which, ultrasonic testing and rebound instrumentation are the most commonly used. For the hollow drum disease, engineers traditionally use a method of tapping to identify its presence, complemented by their extensive experience [1, 2]. These methods are not only time-consuming and labor-intensive, but accurately locating the specific location and area of a disease are also frequently difficult. Most current leakage damage detection methods use direct observation to determine seepage parts and water damage range. Then, an ultrasonic or microwave moisture meter is often used to detect the source of leakage [3, 4]. However, most stone cultural relics have existed for a long time, and the degree of surface weathering is severe. Consequently, signal detection often has difficulty in finding the appropriate detection plane, considerably reducing the accuracy of the detection results. For fissures on or within the surface of a rock, existing detection methods can accurately determine their size and location. For the depth of fissures, however, achieving effective detection of the depth of fissures is difficult. There are a variety of available detection methods such as analyzing rock color, surface layer integrity, mineral composition, chemical composition, and surface hardness, but these methods are qualitative rather than quantitative, and thus, they suffer from difficulty in obtaining accurate mechanical properties of rocks and are prone to bias [5-8].

At present, many scholars mostly have applied ultrasonic detection and the Carsten measuring bottle method to analyze the development degree of the surface hollowing and other diseases of stone cultural relics. In contrast, the application of infrared thermography is less.Therefore, stone cultural relics with surface layers that have different diseases can affect one another and the deterioration trend. In this study, the infrared thermal imaging detection was used to analyze the heat distribution and transfer law of different diseases, and a system based on which was proposed to classify the surface weathering degree of stone cultural relics, which has engineering application value for monitoring and protecting the health status of stone cultural relics.

2. State of the art

Infrared thermography is widely used in various industries worldwide. Swedish scientists began using infrared thermography to detect the thermal insulation performance of buildings in the last century [9]. In the field of construction, the infrared thermography was mostly used to detect internal cracks in concrete, structural defects, and wall voids [10, 11]. However, less research has been conducted

*E-mail address: qinzhongfu@zju.edu.cn
ISSN: 1791-2377
doi:10.25103/jestr.173.09

on the application of the infrared thermography for disease detection in the stone cultural relics field.

In China, the use of infrared thermography for detection has developed rapidly in various industries in recent years. Many scholars have conducted considerable research on the use of infrared thermography to detect diseases in stone cultural relics [12]. For rocks with different water contents under the same heating conditions, Zhang used this technology to detect the water content of the rock surface, temperature change before and after the heating of the rock, and other conditions to verify the applicability of detecting the stone cultural relics' leakage disease [13]. Su et al. used the infrared thermography to monitor the water damage area of stone cultural relics and determined the source of seepage, infiltration pathway, distribution, and activity law [14, 15]. Wu et al. found that infrared thermal imaging technology could effectively detect stalactite covering, flake peeling, and water seepage damage in rock paintings, and the optimal time for its detection varies for different diseases [16]. Huang et al. used the infrared thermography to detect wall cavitation lesions, and they graded the degree of lesions in accordance with temperature inhomogeneity at the defects [17, 18]. Wang et al. used square wave excitation infrared thermography to detect Yuan dynasty wall paintings in Shaanxi and proposed a 3D thermal layer analysis imaging detection method for the hollow drums, cracks, and structural support of the wall [19]. From the perspective of temperature distribution, Zhou et al. performed infrared detection of Chengde Yongyou Temple Summer Resort after the sequencing of the monument, with the help of the change in temperature field within 24 h of the image to analyze its internal fissures and moisture conditions. Then, they measured the monument's internal fissures toward the stability of the monument after its sequencing to provide the basis for the protection of its stability [20]. Su detected the external wall plaster through the filling of water and air preset defects. They found that the larger the area of the hollow drum, the greater the thickness and the effect is more evident. Moreover, the best detection effect was achieved during the morning warming process [21]. In their study of the Northern Wei Dynasty Xuanwu Emperor Jingling underground chamber, Huang et al. determined that the combination of radar and infrared thermal imaging technologies exhibited a good effect on the detection and management of water seepage damage in the chamber [22].

In other countries, Garrido et al. used the infrared thermography to detect moisture in different testing materials [23]. Grinzato et al. analyzed the feasibility of using infrared thermography to detect the disease conditions, such as cavitation and delamination, of frescoes in Italian churches from the perspective of thermal inertia [24]. Biscarin et al. used infrared thermography on Lucano Bridge in Tivoli, Italy to assess its weathering degradation. They investigated the state of weathering degradation of the rock and its causes, proposing a multi-sensing approach for enhanced structural and material degradation assessment [25]. Mineo et al. detected porosity within a rock using infrared thermography. They first heated the rock artificially and then analyzed the cooling curves and cooling rate indices to provide a graphical and numerical representation of the cooling trend. The latter was shown to be strictly correlated with porosity [26]. Milovanovic et al. processed a series of thermograms by using the PCI method to improve the accuracy of infrared thermography for the nondestructive detection of concrete defects [27]. Jo et al. used infrared thermography to conduct a quantitative study of substantial artifact stripping and found that the temperature variation of the rock was most evident at 9:00 a.m. and 10:00 a.m., which were suitable for detection [28]. Avdelidis et al. conducted an infrared inspection of ancient buildings, such as Greek bank walls, before and after restoration. They compared the thermographic results of four different fillers after several months of stone wall reinforcement to assess the protective effect of different restoration materials on the walls [29]. Valluzzi et al. used infrared thermography to nondestructively inspect stone artifacts in Venus and other areas, as well as to detect the condition and effect of restoration [30].

The infrared thermal imaging technology for the single disease detection and disease severity classification of stone cultural relics has begun to be studied and applied in the world. However, the weathering of stone cultural relics is frequently caused by a variety of diseases [31]. With this consideration, the current study draws on the previous classifications for a single class of disease, such as hollow drums and leakage, and selects the Feilaifeng Ligong Pagoda and Huang Ji Tombstone as objects of on-site inspection to summarize the patterns. It aims to create a weathering degree classification system with the amplitude of temperature change of stone artifacts under infrared as an indicator.

The remainder of this study is organized as follows. Section 3 introduces the research methodology, which is primarily a comparison of conventional and infrared detection methods. Section 4 analyzes the infrared detection results and classifies and verifies the weathering grade. Finally, the research results are summarized in Section 5.

3. Methodology

3.1 Cultural relic survey

The Ligong Pagoda in China was built in AD 975, rebuilt in June AD 1587 due to the destruction of floods, and in AD 1590 when Monk Rutong presided over the reconstruction (Fig. 1a). The Ligong Pagoda is located in Lingyin Feilai Peak's Longhong Cave in China. The whole structure is of stone masonry, with six sides and seven stories. It is about 9 m high, and strongly depicts the style of the Ming dynasty Hangzhou. It is the only surviving Ming dynasty pagoda. The overall surface of the Ligong Pagoda is seriously weathered, with water seepage, cracks, hollow drums, and other defects.

The Huang Ji Tombstone in China (Fig. 1b) dates back to the Qing Dynasty Kangxi period, standing for 26 years (1687). The monument body is preserved, but the turtle-shaped pedestal is broken (turtle head). The total height is about 5.2 m, while the width is 1.2 m. The monument is huge, with Manchu and Chinese characters engraved on it. This tombstone has a certain historical research value.

3.2 Conventional detection methods for determining weathering degree on surface of cultural relics

3.2.1 Detection principle

The Castor bottle method is applicable for quantitatively or semi-quantitatively measurement of capillary water absorption and water repellency of a material under a given pressure; it can be used to visually reflect the differences in water absorption capacity of a stone with different degrees of weathering [12].

(a) Ligong Pagoda (b) Huang Ji Tombstone

Fig. 1. Ligong Pagoda and Huang Ji Tombstone.

The moisture meter testing is conducted in a two-stage process: pre- and post-water application, with a half-hour interval in between. A quicker increase in moisture levels between these two points suggests a less compact stone surface, higher porosity, and, consequently, a greater degree of weathering.

The ultrasonic detection is a nondestructive testing method for detecting the density of rock interior in accordance with the characteristics of different propagation speeds of sound waves in various mediums. It can evaluate the surface weathering degree of rocks by integrating the development of various surface weathering features, such as leakage fissures and cavitation. Therefore, this method has reference significance for the classification of the surface weathering grade of stone cultural relics in accordance with infrared thermal image results [13].

3.2.2 Testing equipment

The experimental equipment is provided in Table 1.

Table 1. Field testing instruments.

Wave velocity	Zhong Yan Technology RSM-SY7 ultrasonic detector
Hardness	SNDWAY SW-6210 Leeb hardness tester
Moisture	Moisture meter type MS310
Temperature	FOTRIC C326 thermal imaging camera
Water absorption capacity	Karsten ten tube

3.2.3 Conventional technical testing methods

The ultrasonic tester, hardness tester, Custer bottle and moisture meter were used to detect and record data in the affected areas one by one. The weathering degree of the cultural relics was initially evaluated by the internal wave speed, surface hardness, water absorption performance and other indicators. Then all the previous detected areas were sprayed with water, and about 10 minutes after the water was completely drained. The water absorption index of rock surface is obtained by using the water meter to evaluate the inner density of the rock.

3.3 Infrared detection of weathering degree on surface of cultural relics

3.3.1 Detection principle

Through various types of conventional testing methods, the weathering degree results were presented by different mechanical property indexes in the test area and showed agreement with one another. In accordance with the existing specifications of China for the ultrasonic evaluation of rock weathering degree, the specific degree of rock weathering can be quantified, providing a certain scientific basis for determining the weathering degree of a rock with the temperature drop of the rock under infrared as an index.

3.3.2 Testing equipment

A FOTRIC 326Q handheld infrared camera was used, as shown in Fig. 2. It has a minimum imaging distance of 0.1 m, a temperature measurement range from -20 °C to 650 °C, a high degree of accuracy, and a simple operation that is easy to execute [32, 33].

Fig. 2 FOTRIC 326Q handheld thermal imaging camera.

3.3.3 Infrared thermal imaging detection methods

Passive detection: The detection target does not require heating. Temperature difference detection is carried out only on the target itself, and no external heat source is required. This method is usually used for stone cultural relics detection in the field and open environments.

Active detection: The target is heated before detection. The heating source can originate from inside or outside the object. The difference is detected at this time, resulting in the existence of a large difference in the coefficient of thermal conductivity of the areas. The external energy absorbed by the surface of an object is different from the energy it radiates to the outside. The infrared image will present a large temperature difference. In accordance with the different conditions of the target, infrared detection can be performed at the same time the target is heated. It can also be conducted within a certain period after heating has ended.

Since the stone artifacts were detected on-site, the first detection method was used in this study.

4. Results analysis and discussion

4.1 Moisture content and hardness test results

The water content test data for the three areas of the Ligong Pagoda (A, B, and C) and the Huang Ji Tombstone are shown in Fig. 3. The hardness test data are presented in Fig. 4.

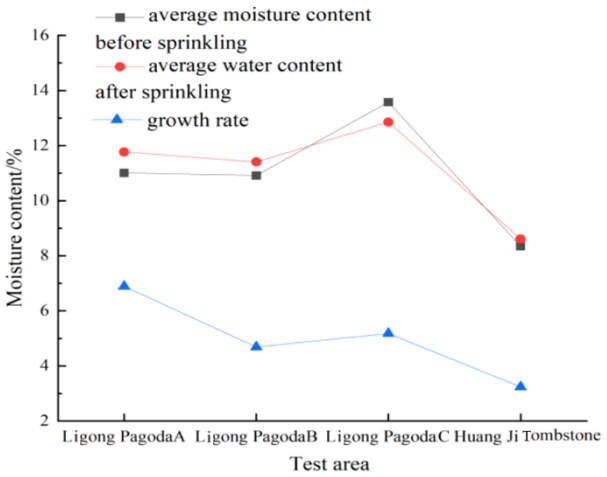

Fig. 3. Moisture content test data

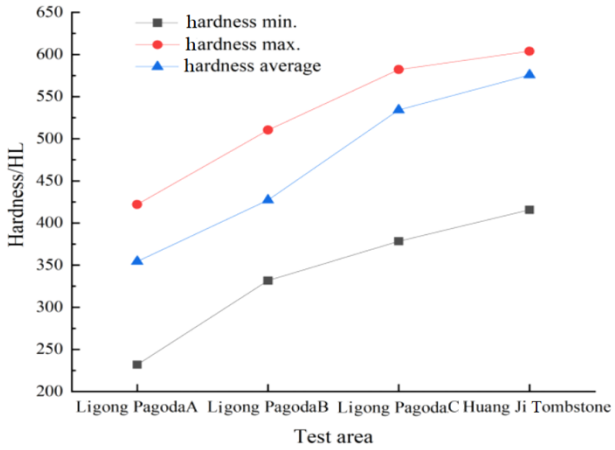

Fig. 4. Hardness test data.

As shown in Figs. 4 and 5, Ligong Pagoda A has high water content, and the growth rate before and after sprinkling is considerably higher than those of the other areas, indicating that the internal porosity of the rock is large, and the material is loose. The surface is darker, with a large amount of calcium sulfate crusts. Ligong Pagoda B has high water content, but the growth rate before and after sprinkling is generally high. The internal material is moderately dense, with low surface hardness. The surface hardness is low, because the long-term high-water content causes rock softening. Weathering degree is medium. Ligong Pagoda C has the highest water content. However, water content exhibits a downward trend after sprinkling water. On the surface of the rock, internal porosity is low and material is dense. Water cannot easily enter the rock's interior. The hardness value is higher, and the weathering degree is low. The water content of the Huang Ji Tombstone is low, and the growth rate before and after sprinkling is low. The hardness value is the highest, indicating that the internal material of the rock is densest, and the degree of weathering is the lowest.

4.2 Test results of water seepage rate

The water infiltration rate test data for the three areas of the Ligong Pagoda (A, B, and C) and the Huang Ji Tombstone are provided in Table 2.

4.3 Ultrasonic test results

In accordance with the experience in the field of engineering geology in WW/T0063-2015 of China, the rock weathering coefficient F_S is used to describe the degree of rock weathering quantitatively in the China Code for Engineering Exploration of Stone Cultural Relic Protection.

The coefficient of rock weathering can be determined using the following formula:

$$F_S = \frac{V_{P0} - V_P}{V_P} \tag{1}$$

where F_S is the rock weathering coefficient, V_{P0} is the compressional wave velocity of fresh rock (m/s), and V_P is the compressional wave velocity of weathered rock (m/s).

Table 2. Karsten ten tube test results

Testing area	Detection time	Data change	Water absorption coefficient/Water absorption capacity	Corresponding weathering levels
Zone A of Ligong Pagoda	10:00-11:10 am	1.8-3.3 mL	1.96/anaerobic water	Strong weathering
Zone B of Ligong Pagoda	10:40-11:10 am	0.1-0.4 mL	0.6/anaerobic water	Moderate weathering
Zone C of Ligong Pagoda	11:25-11:45 am	2.2-2.3 mL	0.2/hydrophobic	Breeze weathering
Huang Ji Tombstone	10:15-11:10 am	3.1-3.2 mL	0.15/hydrophobic	Breeze weathering

The specific evaluation and grading requirements shall be implemented as follows:

Unweather: F_S <0.1; Breeze: 0.1≤ F_S <0.25; Weak weathering: 0.25≤ F_S <0.5; Strong weathering: F_S≥0.5.

The ultrasonic inspection data of the three areas of Ligong Pagoda (A, B, and C) and Huang Ji Tombstone are provided in Table 3.

Note: Given the small surface of the three testing areas of the Ligong Pagoda, the longitudinal wave velocity is the average value of 10 groups of values, while that of the Huang Ji tombstone is the average value of 30 groups of values. The stone samples of the Ligong Pagoda and Huang Ji tombstone were detected as limestone, and the reference longitudinal wave velocity of fresh rock was about 4000–5000 m/s. The same material rocks (Fig. 5) were selected from Feilai Peak slope and brought back to the laboratory after the surface weathering layer was cut. The average longitudinal wave velocity was about 4500 m/s after 30 ultrasonic measurements.

Table 3. Ultrasonic detector results

Testing area	Longitudinal wave speed (m/s)	Weathering coefficient F_S	Degree of weathering
Zone A of Ligong Pagoda	1852	1.43	Strong weathering
Zone B of Ligong Pagoda	2083	1.16	Strong weathering
Zone C of Ligong Pagoda	2658	0.69	Strong weathering
Huang Ji Tombstone	3152	0.43	Weak weathering

Fig. 5. Sample of Feilai Peak rocks

4.4 Thermal image analysis

4.4.1 Thermal image of area A of Ligong Pagoda

As shown in Figs. 6(a) and 6(b), temperature decreases from the cracks and hollow drums to the surrounding area, the temperature in the local area plummets after water sprinkling. The average temperature of 17.06 °C is measured, and therefore, the 17.40 °C isotherm is set.
fissure was faster.

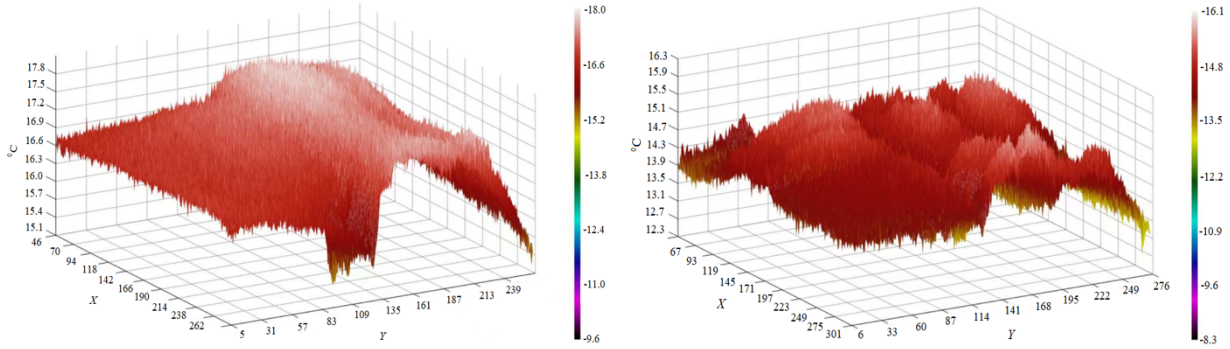

(a) Pre-sprinkling temperature (b) Post-sprinkling temperature

Fig. 6. Pre-sprinkling temperature in Zone A of Ligong Pagoda and Post-sprinkling temperature in Zone A of Ligong Pagoda.

Combined with Fig. 7, the light-colored area (temperature higher than the isotherm) accounted for nearly 40% of the total area. After the region coincided with the surface of cultural relics, it was presumed that there might be hollow drums on the surface of the relics, and the water sprinkler temperature in that region plummeted accordingly.

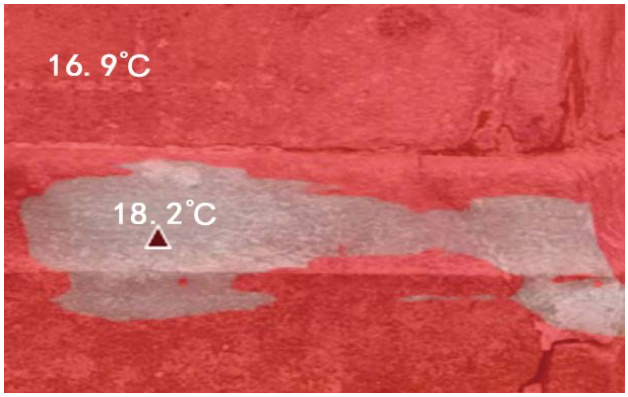

Fig. 7. Cavitation Zone A of Ligong Pagoda

4.4.2 Thermal images of Zones B and C of Ligong Pagoda

Figs. 8(a) to 8(c) show the Ligong Pagoda B and C areas before and after sprinkling. The infrared thermal image reveals the fissures in the Ligong Pagoda B and C areas. The more water, the more serious the leakage through the fissures. The temperature from the fissure to the surrounding area tends to increase. After sprinkling, the temperature drop near the fissure was faster.

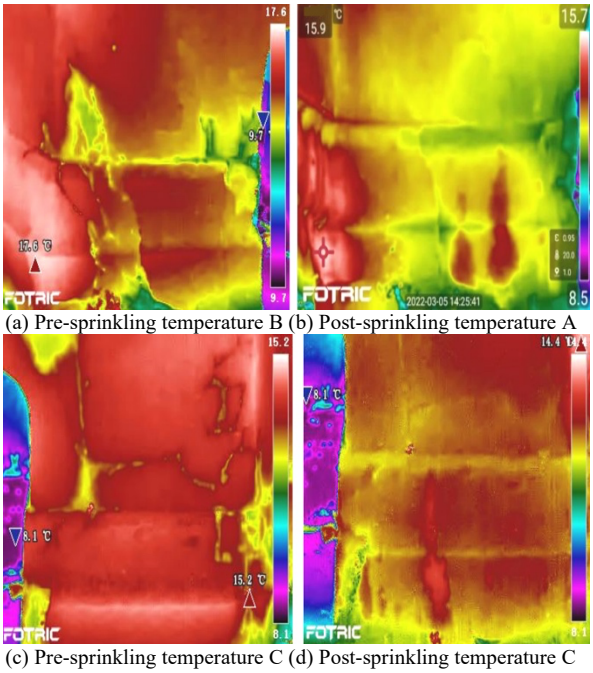

(a) Pre-sprinkling temperature B (b) Post-sprinkling temperature A

(c) Pre-sprinkling temperature C (d) Post-sprinkling temperature C

Fig. 8. Pre-sprinkling temperature in Zone B, Post-sprinkling temperature in Zone A, Pre-sprinkling temperature in Zone C and Post-sprinkling temperature in Zone C of Ligong Pagoda.

Figs. 9(a) and 9(b) show that the development of hollow drums is through the fissure and to the sides. The average temperature of the B area is 15.41 °C. The 15.80 °C isotherm is set up (light-colored). The average temperature of the B area is 15.41 °C. After setting the 15.80 °C isotherm, the area of the light-colored hollow drum is nearly 30%, and the average temperature of the C area is 13.62 °C. After setting the 14.00 °C isotherm, the area of the light-colored hollow drum is nearly 35%.

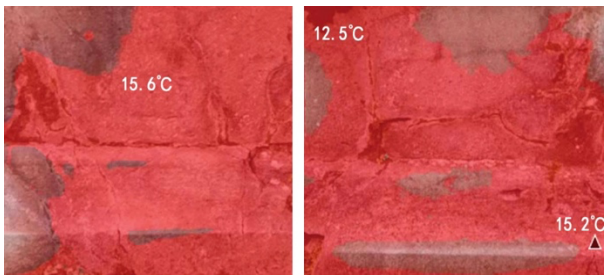

(a) Zone B (b) Zone C

Fig. 9. Cavitation Zone B and C of Ligong Pagoda.

4.4.3 Thermal image picture of Huang Ji Tombstone

As shown in Figs. 10(a) and 10(b), the temperature change of the Huang Ji Tombstone before and after sprinkling water is small.

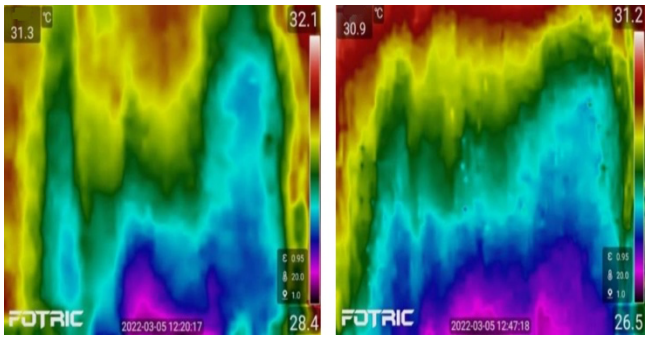

(a) Pre-sprinkling temperature (b) Post-sprinkling temperature

Fig. 10. Pre-sprinkling and post-sprinkling temperature of Huang Ji Tombstone.

Fig. 11 shows that the high-temperature area is less. The surface average temperature is 29.86 °C. After setting the 31 °C isotherm, the high-temperature area is about 5%, because the high-temperature area for the tombstone is located on both sides of the edges and corners. Serious abrasion occurs, and weathering is severe. The internal rock texture exhibits severe osteoporosis, and porosity is higher. Hence, the infrared temperature is higher than the front of the tombstone.

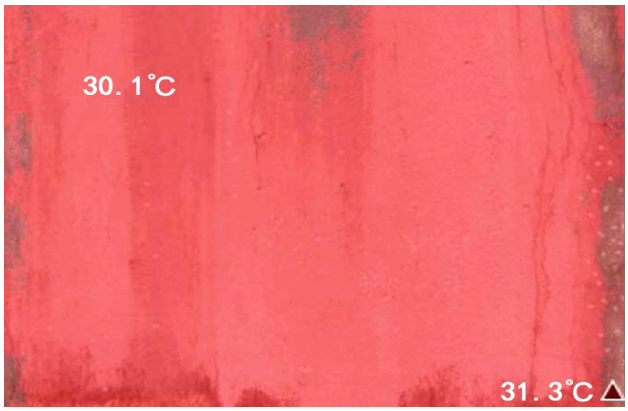

Fig. 11. High-temperature area of Huang Ji Tombstone.

4.4.4 Analysis of data results

Figs. 12(a) and 12(b) show the line graphs of different temperature values before and after watering in the four detection zones. Fig. 12(c) shows the temperature drop before and after watering in the four detection zones.

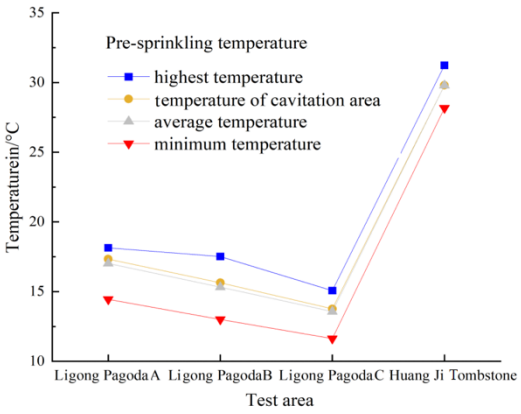

(a) Temperature before watering

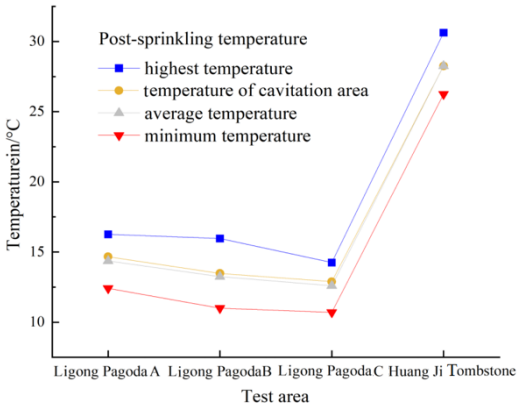

(b) Temperature after watering

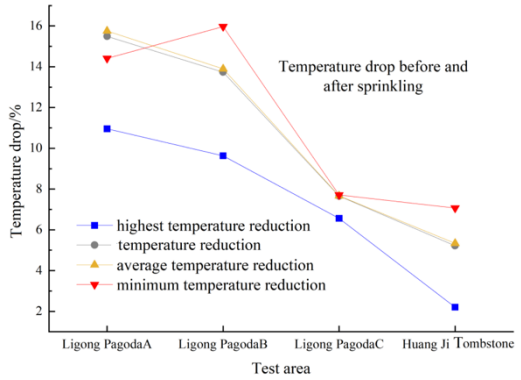

(c) Temperature drops before and after sprinkling

Fig. 12. Temperature before watering, after watering and Temperature drop before and after sprinkling.

As shown in Table 4, the temperature change on the rock surface after sprinkling was approximately 0.30 °C higher than the average in area A, 0.20 °C higher in area B, and 0.25 °C higher in area C. The temperature change of the rock surface before and after sprinkling was also consistent. In addition, the trends of the highest, lowest, and average rock surface temperatures before and after irrigation and the magnitude of the temperature change were the same. The temperature in the hollow drum area is slightly higher than the average temperature and the drop in temperature after sprinkling is even greater. The combination of Figs. to 9 indicates that the hollow drum area on the rock surface covers a significant range. However, except for a few points, the rest of the area is shallow superficial hollow drums that have not developed to depth. Upon analyzing the temperature drop data in Fig. 12(b), the difference between the lowest and highest temperature drops significantly suggests that the leakage damage on the rock surface is more severe than that associated with the hollow drum. Combined

with the infrared image, the leakage damage belongs to fissure leakage.

Table 4. Results compared with conventional detection data

Testing area	Results of routine testing methods	Temperature drops before and after sprinkling
Zone A of Ligong Pagoda	Strong weathering	15.83%
Zone B of Ligong Pagoda	Moderate weathering	13.95%
Zone C of Ligong Pagoda	Breeze weathering	7.76%
Huang Ji Tombstone	Breeze weathering	5.39%

As indicated in Table 5, the weathering degree of rock surface can be preliminarily divided into the following four grades on the basis of the cooling amplitude of stone cultural relics after sprinkling water.

4.5 Evaluation grade verification of weathering degree

According to the research group in the investigation of 87 grottoes (cliff statues) in Zhejiang province, 41 of them are limestone culture relics, 26 of them are tuff culture relics, 10 of them are granite culture relics, 6 of them are rhyolite culture relics, 1 of them are basalt, sandy conglomerate, sedimentary rock, and argillaceous siltstone culture relics.

Table 5. Weathering degree grading of rock surface

Temperature cooling amplitude before and after sprinkling under infrared	Weathering degree
0-5%	Unweather
5-10%	Breeze weathering
10-15%	Moderate weathering
>15%	Strong weathering

Due to the thin section of the tested object being identified as limestone, it has little difference with tuff in many physical performance indicators, to exclude the random test results, so choose another big difference in physical properties of bioclastic micrite limestone qualitative Damaling ridge cliff inscribed for testing to confirm Table 6 stone surface weathering degree of the reliability of the hierarchy.

Table 6. Ultrasonic and infrared testing results of the stone samples inscribed on Damaling ridge cliff

Testing point	Longitudinal wave speed (m/s)	Determination of the weathering coefficient	Temperature drops before and after sprinkling	Degree of weathering
1	1069	0.87	9.40%	Breeze weathering
2	1147	0.74	9.28%	Breeze weathering
3	1211	0.65	8.16%	Breeze weathering
4	1263	0.58	7.83%	Breeze weathering

As indicated in Table 6, the stone samples inscribed on the Damaling Ridge Cliff were bioclastic micritic limestone, and the p-wave velocities at the four measuring points were the average values of 10 groups. Referring to the p-wave velocity of fresh rocks, which is approximately 2000-2500 m/s, rocks of the same material on the nearby hillside were selected and brought back to the laboratory. Once the weathered layer on the rock surface was removed, the mean p-wave velocity, derived from 30 subsequent ultrasonic tests, approximated 2000 meters per second.

The detection results indicate that the weathering coefficient determined by WW/T0063-2015 of China is directly proportional to the cooling amplitude before and after sprinkling on the surface of cultural relics under infrared. The quantitative value is higher, signifying that the weathering degree is more serious. Using the cooling amplitude after sprinkling on the surface of stone cultural relics is feasible as an indicator for determining the weathering degree of cultural relics. However, the rock properties of the two detection objects are different. The differences in physical properties are considerable, and the environmental temperature varies by 2 °C. Therefore, the result exhibits a slight deviation. The Damaling Ridge cliff stone samples in the breeze-weathered category are close to moderate weathering. The judging standard conversion between different materials of a rock remains to be further researched.

5. Conclusions

On the basis of the current specification of ultrasound and by using the infrared thermography for field measurement combined with field ultrasound detection data, the following conclusions were drawn.

(1) The weathering degree of the surface layer of rocks can be classified into the following grades: unweathered 0-5%; slightly weathered 5-10%; moderately weathered 10-15%; and heavily weathered over 15%.

(2) The weathering of stone artifacts typically starts from the corners, which are heavily worn, with higher water content. An increase in water content after sprinkling results in lower hardness, higher temperature detected by infrared, and greater changes.

(3) The lower the longitudinal wave velocity of the rock, the greater the temperature drop before and after watering, i.e., the greater the extent of weathering on the surface of the rock.

The infrared detection is relies on temperature as a reference value, thus, when this detection is performed in spring, the temperature of the rock surface is approximately 15-25 °C. Temperature drop after watering is more related to the initial temperature; therefore, the results of the study do not apply to detection during winter and summer. Further in-depth research is required for a more comprehensive detection.

Acknowledgements

This work was supported by the Zhejiang University Future Academic Star Project (2024-17).

References

[1] J. Huang, Y. Zhang, Y. Zhang, and P. Zhao, "Application of non-destructive testing technique for detecting surface detachment in cultural heritage buildings," *J. Shanghai Uni.(Nat. Sci. Ed.)*, vol. 28. no. 4, pp. 656-667, Aug. 2021.

[2] J. Yang, T. Fan, Y. Yang, and F. Xu, "The research of detection and protection on the stone tower of great Buddha temple in Xinchang," *Stone*, vol. 1, pp. 23-27, Jan. 2014.

[3] C. Ge, L. Ye, S. Wang, H. Jia, S. Li, J. Yang and S. Zhang, "Exploration method of stone statue based on nondestructive testing technology-Taking Xinchang maitreya statue as an example," *J. Eng. Sci. Tech. Rev*., vol. 12, no. 5, pp. 98-103, Sept. 2019.

[4] Z. Zhang, H. Peng, Y. Ma, J. Bai, and X. Ma, "Application of the ultrasonic flawless detector in the preservation of unearthed stony cultural relics," *Int. J. Geomech.*, vol. 11, no. 3, pp. 278-285, Oct. 2005.

[5] L. Ye, M. Fang, Q. Pan, X. Xu, X. Wu, and S. Yuan, "Evaluation on weathering degree of limestone artifacts considering water absorption characteristics," *J. Eng. Sci. Tech. Rev.*, vol. 15, no. 5, pp. 1-8, Nov. 2022.

[6] Y. Fang, J. Zhang, G. Xia, W. Zhou, and M. Su, "Application of infrared thermal imaging on seepage probing of Fengxian temple in Longmen Grottoes," *Geosci.*, vol. 27, no. 3, pp. 750-754, 2013.

[7] P. Luo, S. Wang, P. Hagan, Q. Huang, C. Cao, and K. Gamage, "Mechanical performances of cement-gypsum composite material containing a weak interlayer with different angles," *Dyna*, vol. 94, no. 4, pp. 447-454, May 2019.

[8] S. Wang, P. Hagan, D. Xu, B. Hu, Z. Li, and K. Gamage, "Fracture process and energy dissipation analysis of sandstone plates under the concentrated load," *Mater. Technol.*, vol. 21, no. 6, pp. 1345-1351. Jul. 2014.

[9] M. P. Luong, "Fatigue limit evaluation of metals using an infrared thermographic technique," *Mech. Mater.*, vol. 28, no. 1-4, pp.155-163, Jul. 1998.

[10] G. Luo, J. Pan, and J. Wang, "Infrared thermal imaging technique-based method for detecting defect of insulation layer of concrete dam," *Water Resour. Hydro. Eng.*, vol. 51, no. 12, pp. 71-77, Dec. 2020.

[11] H. Chen, Y. Qin, J. Chen, K. Yao, W. Li, and Y. Tian, "Experimental research on the non-destructive detecting technique on concrete-filled steel tube based on infrared thermal imaging method and ultrasonic method," *Build. Struct.*, vol. 50, no. S1, pp. 890-895, Jun. 2020.

[12] C. Ma, X. Jiang, H. Yan, P. Zhou, J. Ren, Y. Fan, X, Fan and L. Wan, "A study of the formation pattern of condensation water in grottoes based on the infrared thermal imaging technology," *Hydro. Eng. Geol.*, vol. 49, no. 4, pp. 30-36, Jul. 2022.

[13] H. Zhang, "The experimental study on the use of infrared thermal imaging for nondestructive detection of deterioration disease in stone relics," *J. Liaoning Prov. Coll. Commun.*, vol. 15, no. 6, pp. 20-22, Dec. 2013.

[14] M. Su, Y. Fang, W. Zhou, and H. Chen, "Infrared imaging detectionon avalokitesvara condensation water," *Geophys. Geochem. Explor.*, vol. 37, no. 2, pp. 295-300, Apr. 2013.

[15] Y. Fang, J. Zhang, G Xia, W. Zhou, and M. Su, "Application of infrared thermography in water seepage detection in Fengxian Temple of Longmen Grottoes," *Geosci.*, vol.27, no. 3, pp. 750-754, Jun. 2013.

[16] Y. Wu and S. Liu, "Research on infrared thermography detection of seepage damage in petroglyphs," *Sci. Conserv. Archaeol.*, vol. 22, no. 2, May 2010.

[17] Z. Huang, Y. Zhang, Y. Zhang, and P. Zhao, "Application of non-destructive testing technique for detecting surface detachment in cultural heritage buildings," *J. Shanghai Uni.(Nat. Sci. Ed.)*, vol. 28, no. 4, pp. 656-667, Aug. 2022.

[18] Y. Hong, P. Miu, Z. Zhang, S. Zhang, L. Sun, X. Shui, X. Ji and Z. Zhang, "The Ultrasonic infrared thermography and its application in NDE," *J. Nanjing Uni.(Nat. Sci. Ed.)*, vol.39, no. 4, pp. 547-552, Aug. 2003.

[19] C. Wang, N. Tao, Q. Zhang, J. Yan and J. Sun, "Nondestructive detection of murals in Tombs bysquare-Heating thermography," *Acta Opt. Sin.*, vol. 41, no. 16, pp. 1611002, Aug. 2021.

[20] X. Zhou, Y. Fu, and L. Li, "Infrared thermography for Epilogue table of chengde mountain resort," *Nondestruc. Testing*, vol. 37, no. 4, pp. 33-36, Apr. 2015.

[21] J. Su, "Experimental research on infrared technology for detecting plaster defects on building exterior walls," *Guangdong Build. Mater.*, vol. 33, no. 7, pp. 28-30, Jul. 2017.

[22] Z. Huang, Y. Fang, X. Zhang, Q. Dong, Y. Yu, and S. Yan, "GPR/Infrared thermal imaging and its application based on water seepage of underground tomb," *Sci. Technol. Eng.*, vol. 14, no. 10, pp. 140-144, Apr. 2014.

[23] I. Garrido, S. Lagüela, S. Sfarra, F. J. Madruga, and P. Arias, "Automatic detection of moistures in different construction materials from thermographic images," *J. Therm. Anal. Calorim.*, vol. 138, pp.1649-1668, Apr. 2019.

[24] E. Grinzato, C. Bressan, S. Marinetti, P. G. Bison, and C. Bonacina, "Monitoring of the scrovegni chapel by IR thermography: Giotto at infrared," *Infrared Phys. Technol.*, vol. 43, pp. 165-169, Jun. 2002.

[25] C. Biscarini and I. Catapano, "UAV photogrammetry, infrared thermography and GPR for enhancing structural and material degradation evaluation of the Roman masonry bridge of Ponte Lucano in Italy," *NDT & E Int.*, vol. 115, pp. 102287, Jan. 2020.

[26] S. Mineo and G. Pappalardo, "The Use of Infrared Thermography for Porosity Assessment of Intact Rock," *Rock Mech. Rock Eng.*, vol. 49, no. 8, pp. 3027-3039, Aug. 2016.

[27] B. Milovanović, M. Gaši, and S. Gumbarević, "Principal component thermography for defect detection in concrete," *Sensors*, vol. 20, no. 14, pp. 3891, Jul. 2020.

[28] Y. H. Jo, C. H. Lee, and J. H. Yoo, "Study on applicability of passive infrared thermography analysis for blistering detection of stone cultural heritage," *Int. J. Conserv. Sci.*, vol. 29, no. 1, pp. 55-67, Mar. 2013.

[29] N.P. Avdelidis and A. Moropoulou, "Applications of infrared thermography for the investigation of historic structures," *J. Cult. Herit.*, vol. 5, no. 1, pp. 119-127, Jun. 2003.

[30] M. R. Valluzzi and A. Bondi, "Structural investigations and analyses for the conservation of the 'Arsenale' of Venice," *J. Cult. Herit.*, vol. 3, no. 1, pp. 65-67, Jun. 2002.

[31] L. Ye, Q. Li, and P. Sun, "Advances in research on protection of stone relics by science and technology methods," *J. Zhejiang Uni. Sci. Technol.*, vol. 28, no. 5, pp. 394-400, Nov. 2016.

[32] S. Wang, D. Li, C. Li, C. Zhang, and Y. Zhang, "Thermal radiation characteristics of stress evolution of a circular tunnel excavation under different confining pressures," *Tunn. Undergr. Sp. Tech.*, vol. 78, pp. 76-83, Apr. 2018.

[33] S. Wang, C. Li, D. Li, Y. Zhang, and P. Hagan, "Skewed pressure characteristics induced by step-by-step excavation of double-arch tunnel based on infrared thermography," *Teh. Vjesn.*, vol. 23, no. 3, pp. 827-833, Aug. 2016.